Book of Tutorials and Abstracts

European
Microbeam Analysis Society

University of BRISTOL

Mineralogical Society

EMAS 2018

13th EMAS Regional Workshop

MICROBEAM ANALYSIS IN THE EARTH SCIENCES

4 - 7 September 2018

University of Bristol, Wills Hall, Bristol, Great Britain

Organised in collaboration with:
Mineralogical Society of Great Britain and Ireland
and
University of Bristol

THE APPLICATION OF SEM IMAGING TECHNIQUES TO THE STUDY OF RARE FOSSILS

P.J. Orr[1] and S.L. Kearns[2]

1 University College Dublin, School of Earth Sciences
Dublin 4, Ireland
2 University of Bristol, School of Earth Sciences
Wills Memorial Building, Queens Road, Bristol BS8 1RJ, Great Britain
e-mail: patrick.orr@ucd.ie

1. INTRODUCTION

The scanning electron microscope (SEM) is one of the most widely used, and versatile pieces of instrumentation in Earth Sciences research, including palaeobiology. There is a long history of SEM-based imaging of fossils, especially microfossils, for illustrative purposes, taking advantage of the high magnifications and large depth of field possible in SEMs. More recently (in the past 20-25 years) SEMs have become established as a tool for analysing the chemistry of palaeontological materials. Two key technical improvements are especially relevant. The wider availability of environmental (variable pressure (VP) or low vacuum (LV)) SEMs coupled with large volume specimen chambers has allowed macroscopic specimens to be imaged without compromising their integrity, i.e., without cutting them to fit, and/or applying a conductive coating to their surfaces. This has facilitated study of relatively rare materials of sufficient scientific and monetary value that they cannot be destructively sampled.

In particular, SEM analyses of exceptionally preserved, soft-bodied, fossils (Fig. 1) has offered major insights into resolving their taphonomic histories (the processes involved in their fossilisation). This allows the physio-chemical conditions conducive to fossilisation to be elucidated, which, in turn, informs the search for other examples thereof in the geological record. Soft-bodied fossils are preserved principally via two modes of preservation: via authigenic mineralisation, and as organic remains. Mineral infill of voids created by tissues' decay is a third, less common, mode of preservation (Fig. 1A). Replication of tissues in authigenic minerals (almost invariably calcium phosphate) can occur with remarkable fidelity that is often only apparent during SEM imaging (Fig. 1B). Organic remains represent the original tissues, albeit not necessarily the original biomolecules. Organically-preserved examples of decay-prone tissues, e.g., musculature and bone marrow are known (Fig. 1C). However, most tissues preserved in this manner are decay-resistant cuticles e.g. of arthropods and plants (Fig. 1D). These are near two-dimensional due to decay-induced collapse and compaction during burial (carbonaceous compression fossils. Different parts of the fossil, sedimentary matrix, and any authigenic or metamorphic minerals therefore end up juxtaposed over extremely short (micron-scale) vertical distances. SEM-based methodologies have proved to be extremely useful in unravelling these complex mineralogical configurations.

The three techniques principally used are reviewed here:

- secondary electron (SE) images (Figs. 1B and 1C) – to visualise the appearance of the fossil; including charge contrast images (Fig. 1Ea);
- backscattered electron (BSE) images – which express chemical variation in the fossil as greyscale tones (Figs. 1Ad, 1Da and 1Eb);
- energy-dispersive X-ray microanalysis (EDS) – to resolve the fossils' chemistry either as spot analysis (points indicated in Fig. 1Ad) or as X-ray or elemental maps (Figs. 1Ae and 1Ed).

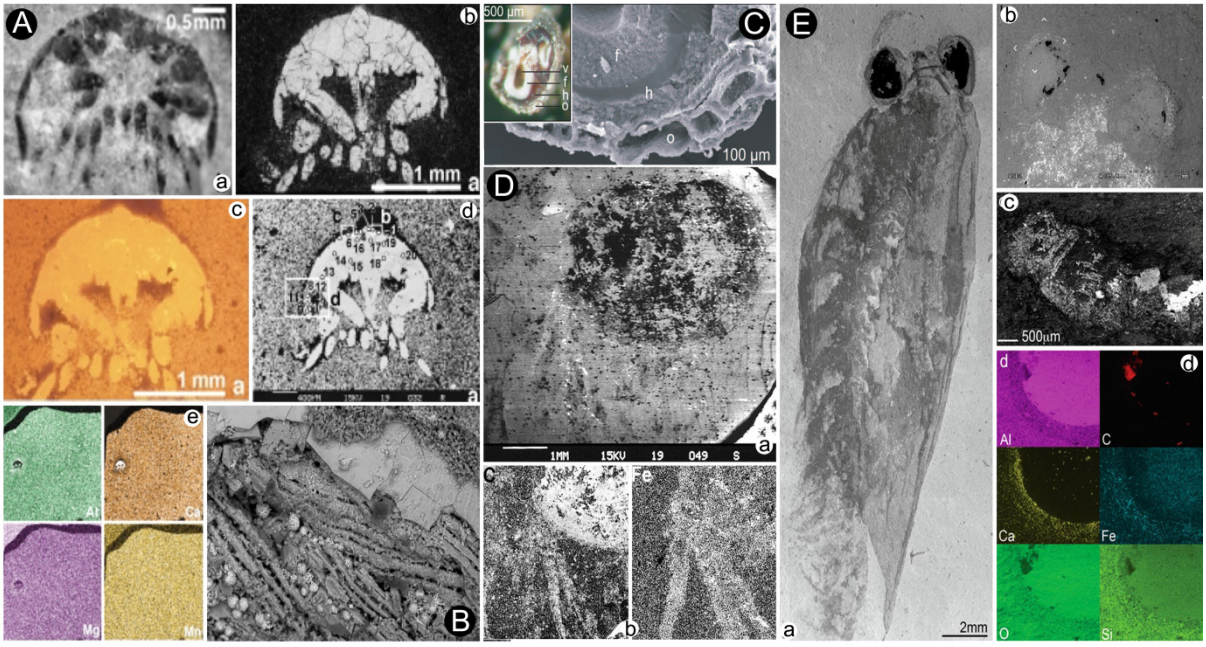

Figure 1. Applications of scanning electron microscopy in the study of exceptionally-preserved 'soft-bodied' fossils. A) Broken surface through arthropod preserved as calcite infill of spaces created by tissue decay (a), and prepared as a polished thin section for optical microscopy (b), cathodoluminescence imaging (c), backscattered electron imaging (d), and X-ray mapping (e) [1] (Orr et al 2000 Geol. Soc. London). B) Secondary electron images of muscle fibres replicated in calcium phosphate (diameter of each 2 - 3 µm). C) Secondary electron images of fossil bone marrow [2] (McNamara et al 2006 Geology). D) Backscattered electron image (a) and X-ray maps for the elements indicated (b) of a near two-dimensional carbonaceous compression fossil [3] (Orr et al. 2008 Palaios). E) Non-destructive imaging and chemical analysis of the Burgess Shale fossil Isoxys sp. (Royal Ontario Museum specimen ROM930912a, b) performed on a single instrument platform. (a) Charge contrast image (see section 3); (b) Backscattered electron image (see section 4); (c) Cathodoluminescence image; (d) X-ray maps for the elements indicated (see section 5). Image from [4].

Each is discussed in turn below. The key concepts and potential applications (and pitfalls) are illustrated with reference to fossil materials, and simulations produced via three pieces of software: (a) Casino (http://www.gel.usherbrooke.ca/casino/), (b) Win X-Ray (https://montecarlomodeling.mcgill.ca/software/winxray/winxray.html), and (c) Electron Flight Simulator (http://www.small-world.net/). These are remarkably useful, user-friendly, tools to explore how the electron beam interacts with samples and the nature of the signals generated.

The review starts with an introduction to a critical concept, excitation and interaction volume, understanding which does much to limit the likelihood of erroneous interpretation of BSE images and the results of X-ray microanalysis. The discussion focusses on the signals generated at accelerating voltages routinely used in the analysis of Earth Science materials (5 - 20 keV). These materials can have different (often complex, even counter-intuitive) behaviours at low accelerating voltages (1 - 2 keV) (see [5]. Thus, some of the comments below re the behaviour of materials do not apply across all accelerating voltages.

Increasingly, SEM instrument platforms incorporate other non-destructive analytical tools (e.g., Raman spectroscopy, cathodoluminescence (CL) imaging), diversifying further the applications of scanning electron microscopy in earth materials research (Fig. 1E). Destructive sampling of extremely small volumes via FIB milling followed by, or increasingly integrated with, SEM-based imaging and chemical analysis of the surfaces produced, is offering unprecedented detail on the ultrastructure of earth materials, including palaeontological specimens.

2. *EXCITATION AND INTERACTION VOLUME*

The electron beam impacting with the specimen generates a series of signals from the surface of and, crucially, inside, the specimen. It is the latter that differentiates any image produced with an SEM from an optical photograph of the surface of a specimen.

2.1. Excitation volume

The term excitation volume is often, but erroneously, used interchangeably with interaction volume. Different signals are derived from different parts of the interaction volume; thus each signal has its own excitation volume. It is the signals generated from these excitation volumes that are used to image the specimen and inform on its chemistry (Fig. 2).

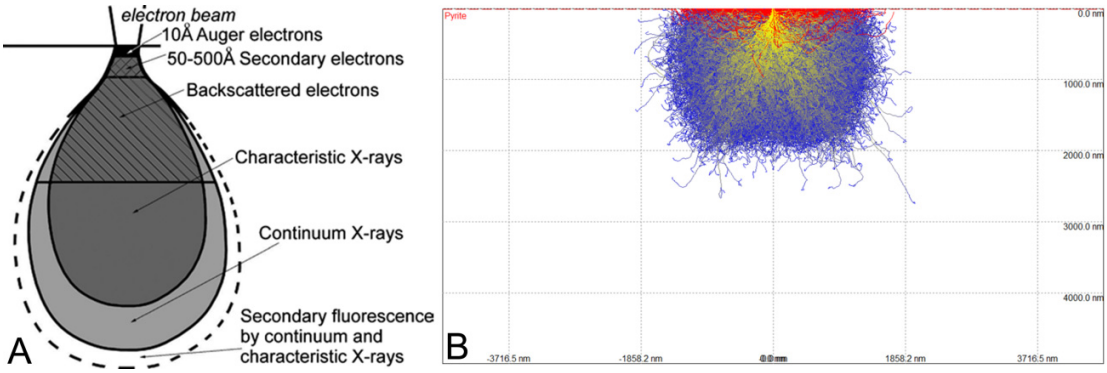

Figure 2. Interaction and excitation volumes. A) The impacting electron beam generates an interaction volume inside the sample, within which each of the various signals generated has its own excitation volume. B) Simulation using Casino of the interaction volume for an accelerating voltage of 20 keV impacting on a FeS_2 substrate, with backscattered electrons shown in red (B). Note that the depth below the surface up to which backscattered electrons are generated is less than that over which electrons penetrate the sample.

2.2. Interaction volume

The size of the interaction volume (and hence each excitation volume) reflects the density, and thus composition, of the material being analysed and the accelerating voltage applied to the electron

beam (Fig. 3). It is especially crucial to bear this in mind when examining natural samples, including fossil material. More than one mineral phase may be present. The composition of the material being analysed is almost invariably complex, spatially heterogeneous, and, of course, unresolved below the surface.

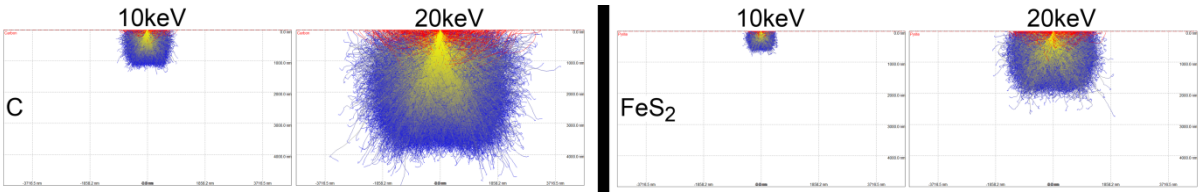

Figure 3. Simulations using Casino of the size of the interaction and excitation volume as a function of composition and accelerating voltage. The size of the interaction volume is larger if the accelerating voltage (keV) applied to the electron beam is increased and the mean atomic number (Z-bar), a proxy for the composition of the material, is less ().

2.3. Surface topography

Surface topography, inevitable in unprepared specimens, will introduce artefacts that impact on the quality of the data. This is the principal reason why analysis of the composition of materials using X-ray microanalysis can only be considered quantitative if the surfaces are flat.

(a) Most obviously, topography can obstruct the path of X-rays or electrons emitted from the sample to the detector; i.e., no signal is detected (shadowing).

(b) Surface topography will also result in markedly different absorption path lengths for X-ray photons (Fig. 4).

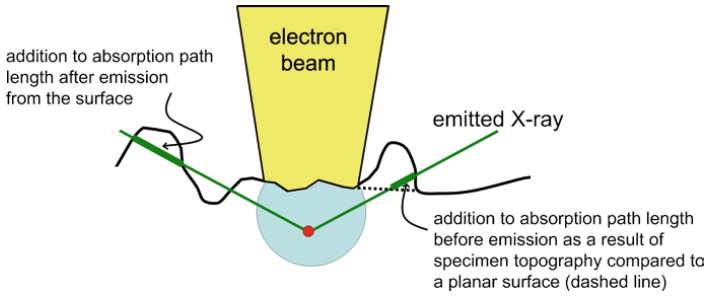

Figure 4. The effect of surface topography on emission of X-ray photons. Relative to a planar surface the total absorption path length can be increased because of topography. The effect can be such that an X-ray photon is fully absorbed and not emitted; thus higher energy photons will be preferentially emitted to be detected.

1.4. Specimen orientation

The orientation of the specimen with respect to the incident beam electrons and the detector is important, i.e., what angle the surface of the specimen is presented at (its tilt). This is not synonymous with the effects of topography. Thus, a perfectly planar surface will not yield the same data if presented at two different angles to the detector (Fig. 5).

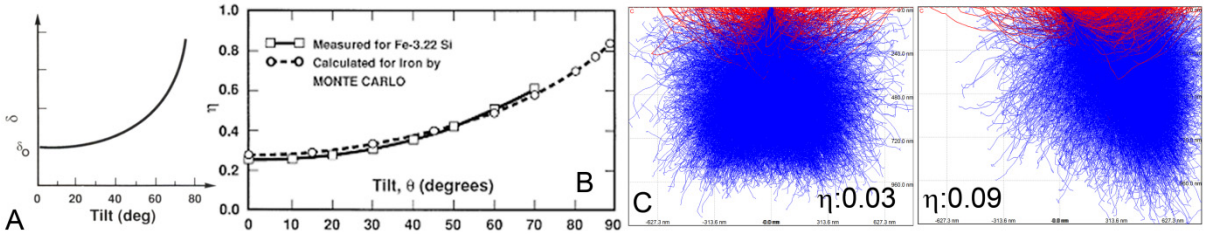

Figure 5. The effects of specimen orientation (tilt) on signal emitted. A) Secondary electron yield (δ), and B) backscattered coefficient value of the backscattered electrons (η) both vary systematically, but non-linearly, as the specimen is tilted (images from [6]). C) Simulation illustrating that the pattern of backscattered electrons emitted is more asymmetrical and the backscattered coefficient greater if the planar surface of the carbon substrate is inclined rather than orthogonal to the electron beam.

3. THE SECONDARY ELECTRON SIGNAL

3.1. Secondary electrons

Secondary electrons are emitted from close to the surface of the specimen and represent electrons loosely bound in the atom; those generated from deeper inside the specimen lack sufficient energy to escape (Fig. 1). Emitted secondary electrons are of low energy (typically < 50 eV).

3.2. Spatial variation

The low energy of secondary electrons means they are relatively insensitive to spatial variation in the composition of the material and rarely express this in the images produced. Some SE detectors will capture backscattered electrons (see below) and may include greyscale tones that express compositional differences. Secondary electrons are primarily used to generate images of the specimen's surface for illustrative purposes (SEI: secondary electron images). The variation in greyscale tone expresses topography, the result of secondary electrons being generated preferentially on features such as ridges and crests and less so in depressions; the former therefore appear brighter. SE yield is higher on sloping surfaces than flat surfaces (Fig. 6). As for all signals emitted from the specimen any obstacle between the signal source and the detector gives rise to shadowing on the image.

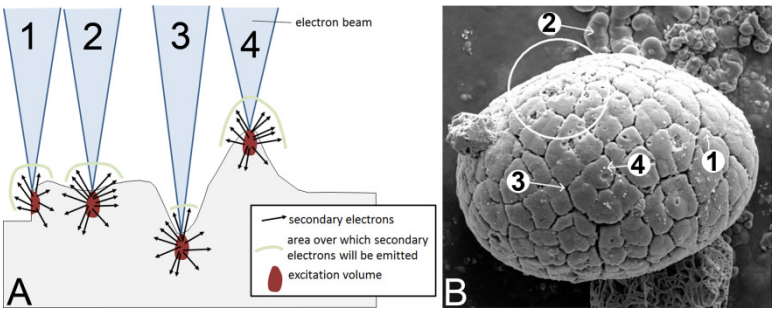

Figure 6. The origin of variation in greyscale tone in secondary electron images (SEI). A) Schematic diagram illustrating how identical secondary electron emission from each excitation volume interacts with topography to produce variation in emission from the sample. Superimposed upon this, the signal detected will also be sensitive to the position of the SE detector. B) A microscopic fossil illustrating how variation in greyscale tone in SEI originates. The fossil's surface is convex, equally so towards the upper and lower edge of the image; the SE detector was positioned to the upper edge of the specimen, thus the fossil's upper face (circled) was facing the detector and is brighter than its counterpart. The edges appear bright (1, in A and B); flat surfaces (2) shows an intermediate greyscale tone. Narrow fissures on the fossil's surface appear black (3); inside these limited secondary electrons were likely generated, and few emitted i.e., these were shielded from the detector. Small raised particles on the fossil's upper surface (4) appear brightest; these are topographic highs, and the path to the SE detector is unencumbered. A) After various sources. B) courtesy of N. Gostling.

4. CHARGE CONTRAST IMAGING

4.1. Charge contrast images

Charge contrast images, a variety of secondary electron image, are a visual representation of the accumulation of electrical charge on the surface of a specimen. Inadequate earthing between specimen and stage prevents impacting electrons dissipating, and results in surface charge accumulating on the surface of the specimen. This results in image drift, electron repulsion and dielectric breakdown, and, almost invariably, deterioration in image quality. Typically, as charge accumulates, the greyscale tone of a secondary electron image increases, often locally obscuring surface detail and rendering the image unusable.

Under high vacuum, surface charge is dissipated by the thin conductive coating usually applied to the surface of dielectric specimens in advance. Under environmental or low vacuum conditions charging is inhibited, and charge neutralisation achieved, by the presence of a gas in the specimen chamber. Interactions between the gas and the electron beam generate positive ions that negate the tendency of negative ions to accumulate on the specimen's surface. The likelihood of the specimen's surface charging can thus be altered by controlling the amount of gas (gas pressure) and type of gas in the chamber. In doing so, the surface of the specimen can be rendered charge negative (all charge is lost to the gas) or charge positive (where charge is held on the sample surface). Crucially, compositional and structural variation over the surface of the specimen can

result in local differences in the extent of any charge trapping. Such images express the amount of charge locally on the surface of the specimen in terms of greyscale tone (charge trapping). The results is a charge contrast image that may define the fossil against the matrix, and/or specific parts of the fossil from each other (Fig. 7).

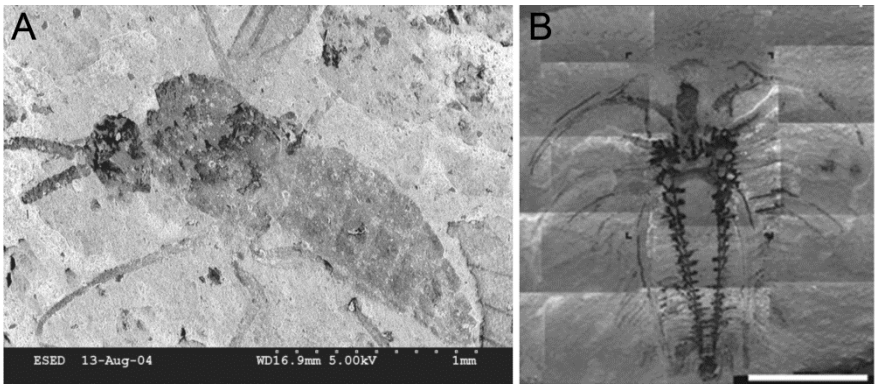

Figure 7. Charge contrast images of palaeontological specimens. A) Charge contrast image of an insect from the Solite Konsevat Lagerstatte preserved as a thin carbon film (confirmed by X-ray mapping see below) (Orr *et al.* in review). The fossil is darker (charging less) than the matrix. The fossil is reasonably uniform in its greyscale tone, with the wing veins and parts of the head and thorax (where the cuticle is thicker) slightly darker. Compare with the backscattered electron image of counterpart in Fig. 10. B) Specimen of Marrella splendens from the Burgess Shale Formation. From [8].

The methodology has been widely used by material scientists, for example, to detect compositional variation in zoned minerals. It has been less widely used by palaeobiologists, but has potential as an alternative to both SEI and BSE imaging. Carbonaceous compression fossils are likely to be particularly suitable given the contrast between the naturally conductivity of the fossil and the almost invariably dielectric siliciclastic or carbonate rock matrix. Surface variation in composition is not, however, the only cause of differential charge accumulation on the surface of a specimen. Topography can be important with charge often preferentially accumulating on raised edges.

4.2.

It is difficult *a priori* to predict the conditions that will generate charge contrast images for a specimen, and these will vary between different materials. It is likely that similar materials may generate charge contrast images under approximately the same operating conditions. It may be useful, therefore, to record the instrument settings that yield any charge contrast images if analysing multiple specimens: the gas pressure inside the chamber (Pa) plus the accelerating voltage, working distance, beam current, scan speed and conditions used for digital imaging.

Modifying the gas pressure inside the chamber, beam current and changing keV are the principal variables the user has control over, and the impact of doing so should be investigated first.

4.3.

Unlike backscattered electron images (see below) the greyscale tone in charge contrast images does ***not*** necessarily reflect the material's composition (Fig. 8).

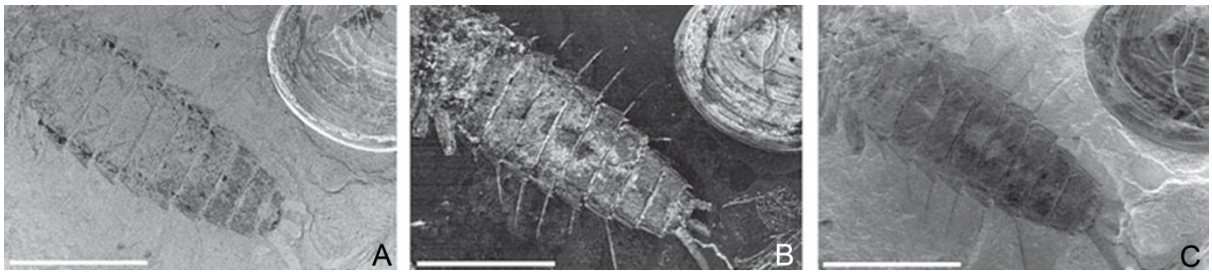

Figure 8. SEM images of fossils from the Jehol Biota, Cretaceous, China. A) Backscattered electron image; note the difference in greyscale tone between the carapace of the conchostracan Eosestheria (brighter: upper right) and the insect carapace. The dark tones of the latter suggest a carbonaceous composition but this can only be proven by X-ray micro-analysis (see below). B and C) Charge contrast images: note that in each image both fossils, despite being compositionally different, are a similar greyscale tone, and that by altering the operating conditions (a combination of gas pressure inside the chamber, beam current, scan speed and image acquisition conditions) the fossils can be made to charge more than (B) or less than (C) the matrix.

5. BACKSCATTERED ELECTRON IMAGES

5.1.

Backscattered electrons, as their name implies, are incident electrons from the electron beam that are reflected back from within the excitation volume as a result of elastic scattering interactions with specimen atoms. Their energy is greater than secondary electrons and they generally travel in straight lines, as a result of which a wide angle detector is required for signal detection.

Although backscattered electron images of unpolished surfaces do contain data on the topography of a specimen, their principal use is to inform on its chemistry.

The energy with which the electrons are backscattered is a function of the mean atomic number of the material impacted (Z-bar), which in return relates to its composition. It is this relationship that is exploited in BSE images; the Z-contrast is expressed in greyscale tones, and phases with higher Z-bar appear brighter (Fig. 9). Most minerals are a mixture of several elements, and thus there is not necessarily a unique Z-bar for each. Composition should not be assumed on the basis of greyscale tone in a BSE image, nor differences in composition inferred from differences in greyscale tone between two images. Greyscale tone can, for example, be altered simply by altering

brightness and contrast in any digital image either at the time of acquiring it, or afterwards via imaging processing software. Determining composition requires x-ray microanalysis of the material (see below). Z contrast should not be confused with backscattered coefficient (η: see below).

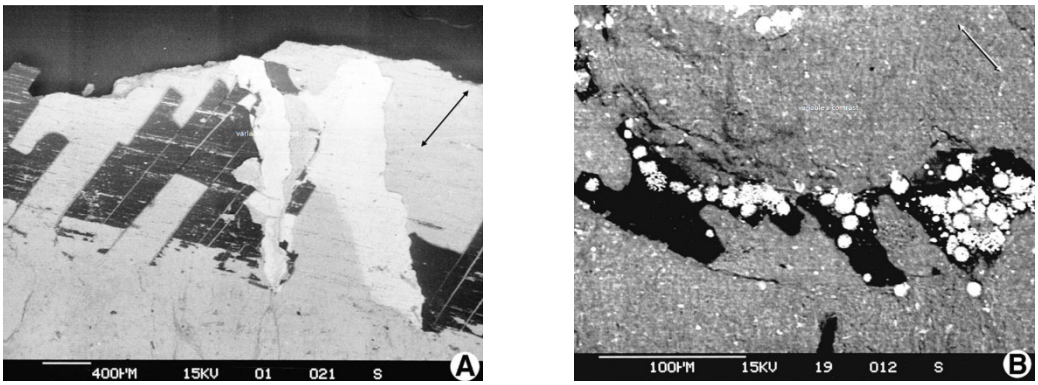

Figure 9. Backscattered electron images showing common rock forming materials. Carbon (Z = 6) preserving plant material (A) and the cuticle of an arthropod (B) is typically black in BSE images, and silicate and carbonate phases, various shades of grey. S ulphide minerals (e.g., pyrite as herein, sphalerite) often appear brightest; the atomic numbers of Fe and Zn are 26 and 30 respectively. Images from [9].

5.2.

The size of the interaction volume, and thus the excitation volume for backscattered electrons, will vary depending on operating conditions, most notably accelerating voltage and the composition of the material being analysed (Fig. 1). It is *essential* to remember that the backscattered electrons are sourced from a volume of material, not just that exposed at the surface. The case study in Fig. 10 illustrates this. The impact of variation in composition with depth can be minimised by lowering the accelerating voltage (albeit with the attendant problem of generating sufficient signal).

5.3.

The backscatter coefficient (η) is a numerical value that ratios the number of backscattered electrons (n_{BSE}) to the number of number of incident electrons (n_B); $\eta = n_{BSE} / n_B$. η is therefore always < 1. Below around 2 keV the relationship between η and keV is complex; see [5] for further discussion. The following statements apply to accelerating voltages above 2 - 5 keV.

Figure 11 plots η values against keV for the following: pure SiO_2; pure C; films of C (thickness in microns (µm) indicated) on top of a SiO_2 substrate. This mimics the structure of the carbonaceous compression fossil exposed on the surface of a siliciclastic matrix in Fig. 10B. Note the following indicated by numbering on Fig. 11, and those scenarios exhibited by the fossil in Fig. 10B.

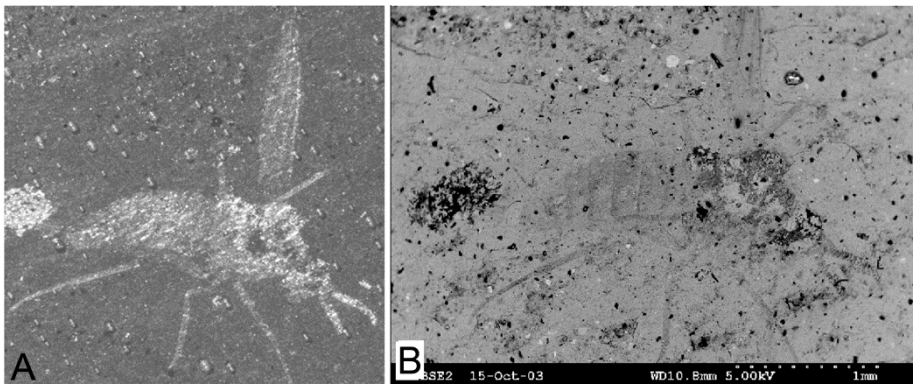

Figure 10. Optical photograph (A) and backscattered electron image (B) of the counterpart of the insect shown as a charge contrast image in Fig. 7A. X-ray mapping (see below) confirms it is preserved as a carbon film (carbonaceous compression), graphitised by metamorphism (hence its being uniformly reflective under incident light (A)). In the backscattered electron image the head and thorax are a combination of bright tones and very dark tones, while the abdomen is almost the same greyscale tone as the matrix. The brightest tones are metamorphic biotite that formed only where the cuticle was thickest (hence its association with the dark coloured areas where the carbon layer is thicker). The surficial carbon film in the abdomen of the fossil is so thin that even at 5 keV most of the backscatter signal is derived from the underlying matrix, hence its being a greyscale tone intermediate between the matrix and the fossil.

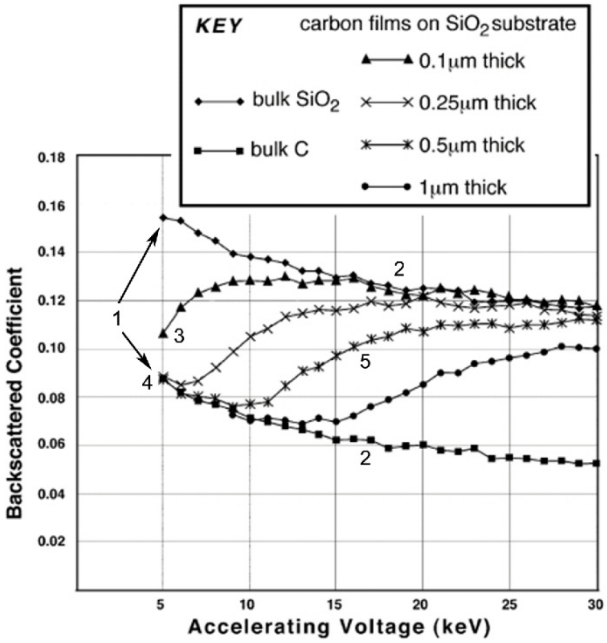

Figure 11. Simulations using Electron Flight Simulator of the relationship between backscattered coefficient and accelerating voltage for the materials indicated in the key. After [9].

[1] η increases with Z monotonically, thus η is greater for SiO_2 than C for all keV values; in Fig. 10B, the fossil is darker than the matrix, consistent with this (but not, on its own, proving the actual composition of either).

[2] As keV is increased η decreases for both SiO_2 and C. For many rock forming minerals η decreases as accelerating voltage is increased; as the excitation volume increases, proportionally more of the signal is generated at depth and the number of emitted backscattered electrons decreases.

[3] Even at 5keV η for a 0.1 μm carbon film on a SiO_2 substrates is between that for SiO_2 and C; i.e., there is a contribution to η from both the carbon film and the underlying SiO_2.

[4] All the other carbon films behave as bulk carbon at 5 keV i.e., the excitation volume is contained solely inside the surficial carbon layer.
In Fig. 10B the backscatter signal for the abdomen (behaving as 3) and thorax/head of the insect (behaving as 4) vary because of differences in the thickness of the cuticle.

[5] For these carbon films η increases as keV is increased; ultimately most have η values at or near that for SiO_2; i.e., progressively more and ultimately most/all of the signal emitted is from within that part of the excitation volume below the surficial carbon layer.

5.4.

Carbonaceous compression fossils can comprise multiple layers of carbon juxtaposed on the surface of the plane of splitting. This produces lateral variations in the thickness of the fossil corresponding to different parts of the anatomy. As illustrated in Fig. 12 the relationship between Z and keV can be exploited to 'tease apart' the separate layers and image them.

6. X-RAY MICROANALYSIS

6.1.

X-ray microanalysis is used to inform on the mineralogy of specimens. Element or X-ray mapping of unprepared fossil specimens embedded in matrix is, as a result of improvements in instrumentation over the past twenty years, increasingly widely used; notably, improvements in X-ray detectors (principally, the SDD-EDS detector) allow greater X-ray throughputs to be used, thus improving the efficiency of the mapping (Fig. 13). Such maps yield qualitative data on the distribution of elements analysed for over a user-defined area. In summary, an area (typically a square or rectangle) is mapped by stepping the stage or electron beam through a series of x,y co-ordinates at each of which an analysis is performed. The data collected is displayed as a series of images in which the greyscale tone is relative to the abundance of that element: the 'maps'. Orr and Kearns [4] provide further information.

All the principles and many of the caveats discussed below also apply to analysis of composition via single point analysis (presented as either an X-ray spectrum or tabulated data) or line scans.

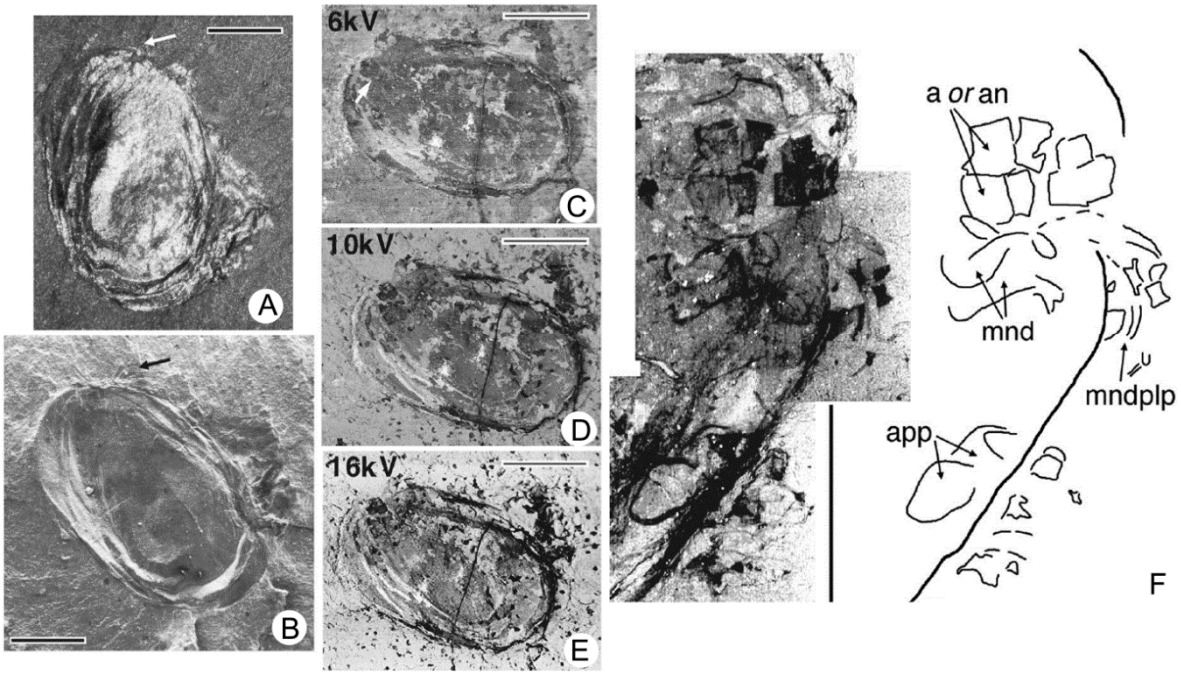

Figure 12. Backscattered imaging used to reveal appendage detail in an ostracod fossil. The carbonaceous carapace overlies the appendages, which are therefore only apparent in an optical photograph (A) and secondary electron image (B) where they project beyond the carapace outline (at arrows). The more proximal parts of the appendages below the carapace are revealed in BSE images at 10 keV (D) and especially 20 keV (E, F), but not 6 keV (C). At 6 keV the excitation volume is contained solely in the carapace. However, in the other BSE images part of the (larger) excitation volume extends below the carapace. It thus samples either the underlying matrix or where locally present, the appendages; the latter are carbonaceous thus Z-bar is lower.

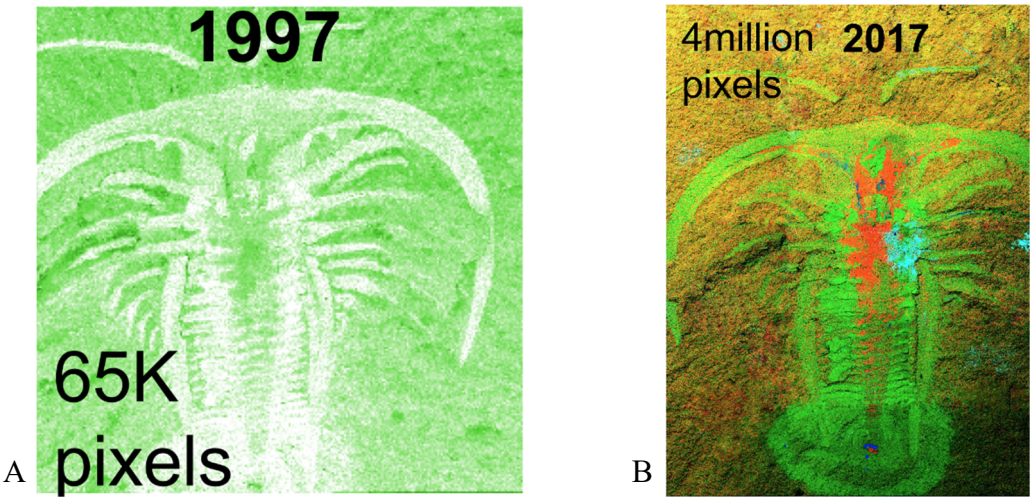

Figure 13. Comparison of X-ray maps generated in 1997 and 2017 for the same specimen of *Marrela splendens* from the Burgess Shale (Middle Cambrian) Canada. A) In 1997 acquired on a Si(Li) EDS detector, each image requires a region of interest on the ED spectrum to be selected resulting in 8-bit maps of a single element. B) Modern acquisition on SDD system where every pixel contains a full EDS spectrum and can then be processed by complex multivariate statistical packages to reveal complex phase distribution.

Most SEM systems employ an energy-dispersive X-ray spectrometer as the detector (all the X-ray spectrum is collected simultaneously: referred to as an EDS or EDX spectrum). The alternative is a wavelength-dispersive X-ray spectrometer (WDS or WDX: a single detector collects a specific part of the spectrum; multiple detectors on the instrument usually an EPMA ensure the full spectrum is collected).

6.2. X-ray generation

The following is a brief (and somewhat simplified) review of how X-rays are generated. Its principal purpose is to explain the origin of the nomenclature used to identify the characteristic lines, and from that the elements present; Reed (appendix 2 in [10]) provides further information.

An atom can be modelled as a nucleus around which electrons orbit in a series of shells. We will consider the inner atomic electron shells (K L and M); note that L and M comprise 3 and 5 subshells, respectively. The impacting electron beam causes the ejection of an electron from one of these electron shells (Fig. 14A) from inside the interaction volume (Fig. 14B). Inner shell ionisation occurs when a tightly bound inner shell electron is ejected; the atom returns to ground state via either the production of an Auger electron or an electron from an outer shell falls into the inner shell in the process of which X rays are emitted (Fig. 14A), to be 'collected' by a suitable detector.

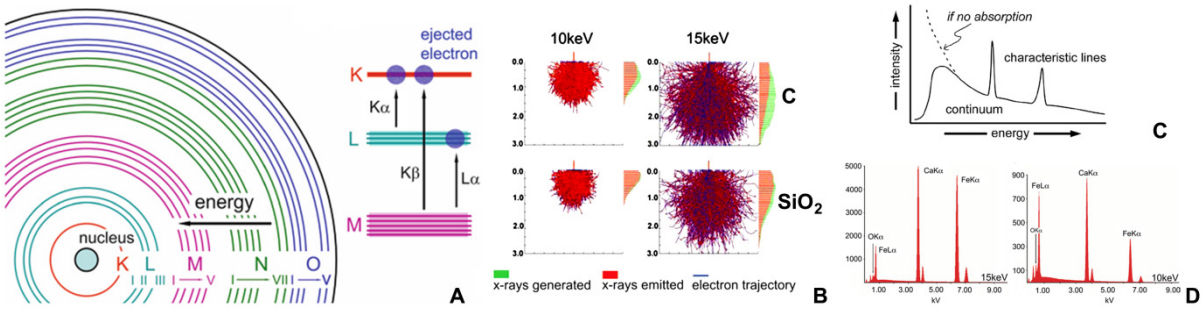

Figure 14. Principles of X-ray generation and structure of an EDS spectrum. C, after Reed ([10] Fig. 2.6).

The data gathered is displayed visually as an EDS spectrum which plots energy of the X-ray against counting intensity (Figs. 14C and 14D). The ED spectrum comprises multiple peaks (characteristic lines) above a background. The latter is the 'continuum' or 'bremsstrahlung'; its asymmetrically convex upwards shape is typical, demonstrating how it varies with X-ray energy (Fig. 14C). The 'continuum' or 'bremsstrahlung' makes characteristic lines of low intensity difficult to detect. Their low intensity may originate because that element is present in low abundance but is also highly sensitive to the operating conditions chosen (see below).

The notation (Siegbahn) traditionally used to describe the characteristic lines, e.g., $K\alpha_1$, comprises three parts. K L or M indicate which inner shell was ionised (i.e., 'lost' an electron). The first suffix e.g., α, β, groups characteristic lines for that shell on the basis of their having a broadly similar intensity. The number sequence in the second suffix orders reflects the sub-shells. The energy of the characteristic X-ray is the difference in energy between the levels involved. In many cases X-rays emitted with very similar energies effectively form one peak in EDS spectrometers and are referred to by just the first two terms: e.g., Fe-Kα (6.4 keV) comprises Fe-$K\alpha_1$ (6.40384 keV) and Fe-$K\alpha_2$ (6.39084 keV).

The combination of characteristic lines is specific for each element. However, individual characteristic lines for different elements can have similar energies. Automatic identification of which elements are present by the operating software may be available but is not fool proof. Identification of which element is present from a single characteristic line can be difficult, especially if operating conditions reduced peak resolution.

6.3.

The structure of the ED spectrum relates to the composition of the sample, the operating conditions, specifically accelerating voltage, and the principles of X-ray generation outlined above. For most systems the user will have control over the instrument variables e.g., accelerating potential and beam current which will control the count rates and dead time of the ED system. It is possible to adjust the amplification time that may reduce dead time at the expense of poorer energy resolution. These issues are not discussed further here, but care should be taken to ensure these are optimised for the objectives of the analysis.

The relative heights of the characteristic X-rays will vary depending on accelerating voltage (Fig. 14D). Only a limited number of characteristic lines may be generated, for example if operating at low accelerating voltage (see 6.3). The effects of specimen topography are more pronounced for lower energy X-rays. Finally, operating under low vacuum conditions to inhibit specimen charging presents specific challenges to accuracy of analyses (see 6.4).

The electron beam will penetrate the sample further, and thus the excitation volume and interaction volumes will be larger, the higher the accelerating voltage and the lower the Z-bar (Fig. 3). Layered substrates present a particular analytical challenge, especially if the surficial layer has low mean Z (e.g., is carbonaceous); at higher accelerating voltages it is possible to render this layer essentially invisible to the x-ray detector (Fig. 15;).

The intuitive solution is to operate at as low an accelerating voltage as possible, but this presents its own challenges. Firstly, to cause the ejection of an electron, the critical excitation energy must be exceeded, i.e., the energy of the incident electron must exceed that binding the electron in the shell to the atom's nucleus. In short, the accelerating voltage chosen must be appropriate to

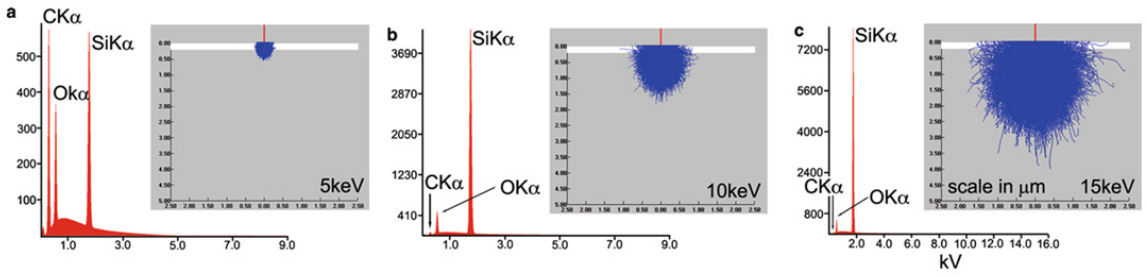

Figure 15. Simulated ED spectra (using Win X-Ray) at the accelerating voltages indicated for a surficial layer of carbon on a silica substrate. At 10, and especially, 15 keV the characteristic line for C-Kα is subsumed within the continuum, as most of the interaction volume occurs deeper in the specimen and the contribution of the carbon layer to the total emitted X-rays is negligible.

generate sufficient x-rays for analysis. The voltage chosen (E_o) must exceed the ionisation energy of the characteristic X-ray in question (E_i). For example, Fe-Kα has an energy of 6.4 keV and Fe-Lα, 0.7 keV. Thus, at an accelerating voltage of 15 keV, both Fe-Kα and Fe-Lα X-rays will be generated, but only the latter at 5 keV (Fig. 16). Further, it is necessary to generate enough X-rays (counts); note the increase in height of the Fe-Kα characteristic line between 10 keV and 15 keV in Fig. 16. The overvoltage ratio should therefore ideally be around 2 or more, i.e., at an accelerating voltage of 15 keV or 20 keV sufficient X-rays will be generated with energies up to around 10 - 12 keV; in Fig. 16 note the fall off in counts as each spectrum approaches the energy of the accelerating beam.

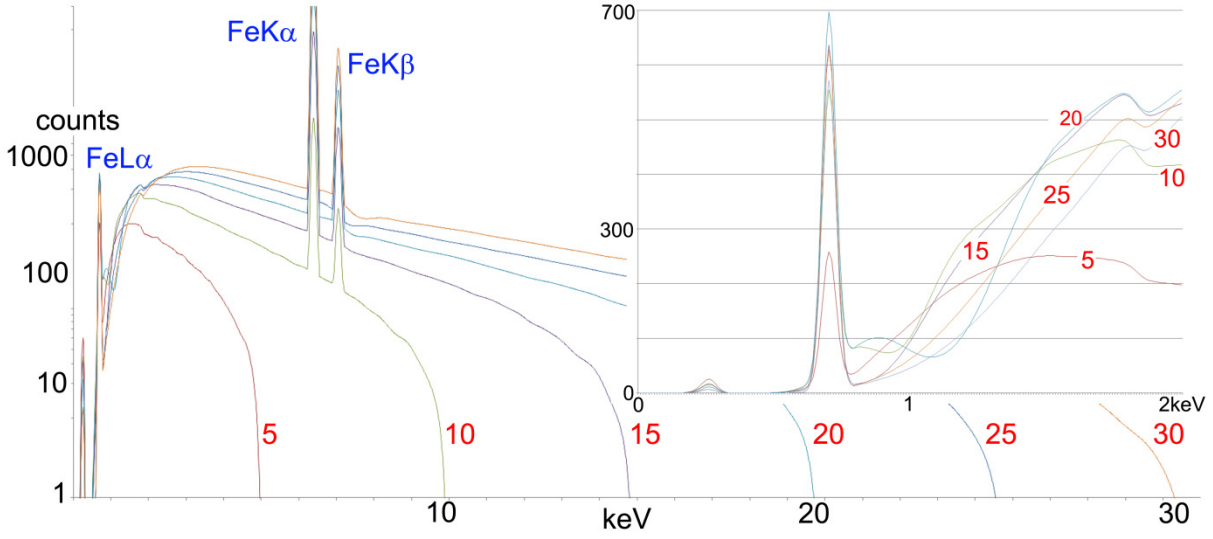

Figure 16. Simulations (using Win X-Ray) of count rates versus X-ray energy (in keV) for an Fe substrate analysed with an electron beam at the accelerating voltages indicated (in red). Note: axes in main image are log-normal.

Secondly, inner shell ionisation of more tightly bound electrons occurs less frequently, thus proportionally fewer higher energy X-rays are generated. Increasing the accelerating voltage will generate more of these X-rays: note the increase in counts with accelerating voltage at the right hand side of each spectrum in Fig. 16. However, proportionally more of the signal is now being generated deeper inside the sample and lower energy X-rays will be preferentially absorbed (in Fig. 16 the counts for the Fe-Lα characteristic line increase from 5 - 20 keV but decreases afterwards). The relationship between X-ray energy and absorption is extremely complex and non-linear (see [10]). In general, lower energy X-rays are thus more likely have been sourced from closer to the specimen's surface, i.e. the upper parts of the interaction volume.

If operating at low voltages it may be possible to analyse using the Kα-lines for light elements (e.g., C, O) but for many other elements a lower energy line will be used e.g. e.g., at 5 keV, X-ray maps for Fe would require analysis of data collected from the Lα-line (Fig. 16). Alternatively, repeat analyses at different accelerating voltages to ensure comprehensive understanding of a specimen's mineralogy, although bear in mind the potential complications that result from changing the size of the interaction volume.

6.4.

X-ray microanalysis under low vacuum conditions may be desirable (for example to prevent surface charging of an uncoated specimen) but presents a particular challenge. The presence of a gas in the specimen chamber results in beam scattering; the effect varies between different gases. As a result of beam scattering, X-rays are generated from a much larger volume than would be the case under high vacuum conditions. The EDS spectrum generated includes a contribution from 'stray x-rays' peripheral to the area of interest (typically positioned under the cross hairs before analysis) (Fig. 17).

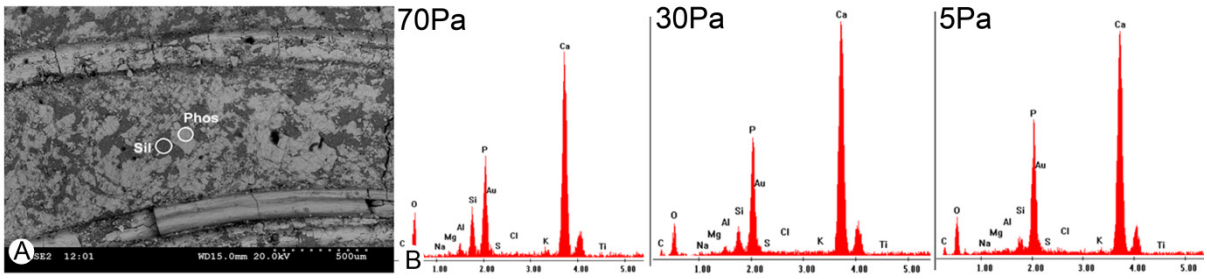

Figure 17. Impact of beam scattering on X-ray microanalysis as a function of gas pressure inside the specimen chamber. A) Fossil fish the scales of which are preserved in calcium phosphate (labelled Phos: bright tones in the backscattered electron image) in a siliciclastic sediment matrix (Si: darker tones). B) EDS spectra for spot in A labelled 'Phos'; note that as the gas pressure in the chamber is reduced (i.e., higher vacuum conditions) the peak for Si-Kα becomes smaller, as the surface area below which the X-rays are being generated contracts as the beam skirt reduces. Note that even at a chamber pressure of 5 Pa the contribution from the Si persists.

7. REFERENCES

[1] Orr P J, Briggs D E G, Siveter D J and Siveter D J 2000 Three-dimensional preservation of a non-biomineralized arthropod in concretions in Silurian volcaniclastic rocks from Herefordshire, England. *J. Geolog. Soc.* **157** 173-186

[2] McNamara M, Orr P J, Kearns S L, Alcalà L, Anadón P and Peñalver-Mollà E 2006 High-fidelity organic preservation of bone marrow in ca. 10 Ma amphibians. *Geology* **34** 641–644

[3] Orr P J, Briggs D E G and Kearns S L 2008 Taphonomy of Exceptionally Preserved Crustaceans from the Upper Carboniferous of Southeastern Ireland. *Palaios* **23** 298-312

[4] Orr P J and Kearns S 2011 Chapter 11. X-ray microanalysis of Burgess Shale and similarly preserved fossils. in: *Quantifying the evolution of early life. Numerical approaches to the evaluation of fossils and ancient ecosystems*. (Laflamme M, Schiffbauer J D and Dornbos S Q; Eds.) (Heidelberg, Germany: Springer, Topics in Geobiology 36) 271-299

[5] Wuhrer R and Moran K 2016 Low voltage imaging and X-ray microanalysis in the SEM: Challenges and opportunities. *IOP Conf. Ser.: Mater. Sci. Engng.* **109** 012019

[6] Goldstein J I, Newbury D E, Echlin P, Joy D C, Romig A D Jr, Lyman C E, Fiori C and Lifshin E 1992 *Scanning electron microscopy and X-ray microanalysis: A text for biologists, material scientists, and geologists; 2nd edition.* (New York, NY: Plenum Press)

[7] Orr P J, Kearns S L, Briggs D E G, Fraser N C, Beard J S, Johnson D, Kilburn M R and Wade J 2018 Taphonomy of the Late Triassic Solite Konservat Lagerstätte and implications for Burgess Shale-type preservation. *Palaeontology* (under review)

[8] Kearns S L and Orr P J 2009 Charge contrast imaging of exceptionally-preserved fossils. *Palaeontology* **52** 663- 680

[9] Orr P J, Kearns S L and Briggs D E G 2002 Backscattered electron imaging of fossils exceptionally preserved as organic compressions. *Palaios* **17** 110-117

[10] Reed S J B 1996 Electron microprobe analysis and scanning electron microscopy in geology. (Cambridge, UK: Cambridge University Press)

[11] Orr P J, Kearns S L and Briggs D E G 2009 Elemental mapping of exceptionally preserved "carbonaceous compression" fossils. *Palaeogeography, Palaeoclimatology, Palaeoecology* **277** 1-8